Reaction mechanisms at the homogeneous–heterogeneous frontier: insights from first-principles studies on ligand-decorated metal nanoparticles

Manuel A. Ortuño * and Núria López *

The frontiers between homogeneous and heterogeneous catalysis are progressively disappearing. The decoration of transition metal nanoparticles (NPs) with ligands, also known as surface modifiers or capping agents, primarily allows NP size control but dramatically impacts activity and selectivity in catalysis. Computational tools have shown their capability of providing insight at atomic level in both homogeneous and heterogeneous areas but, due to the complexity of these interfaces, the underlying reaction mechanisms are often not described and certainly not well understood. In this mini-review, we describe the main challenges in modelling and survey the most recent computational studies that emphasise the role of ligands in tuning catalytic performance. We focus on density functional theory (DFT) simulations of the interfaces between transition metals (ruthenium, palladium, platinum, gold) and organic ligands (NHC, amine, phosphine, thiol), surfactants, and ionic liquids. Revealing the reaction pathways that operate at this hidden interface between homogeneous and heterogeneous worlds will provide guiding rules to design new systems that circumvent linear scaling relationships and foster a unified theory of catalysis.

1. Introduction

Much before the advent of nanoscience, catalysis was one of the areas where small metal structures, either alone or modified by organic moieties, were most widely employed. In particular, metal nanoparticles (NPs) outstand in catalysis[1,2] due to their surface/volume ratio and nanometric size, which grant them unique catalytic properties at the frontier between bulk materials and molecules. Nowadays, although controlling the size and shape of metal NPs has been achieved with a high degree of control,[3–7] the surface functionalization[8] by ligands can further enhance and fine-tune the catalytic performance by merging the versatilities of both heterogeneous and homogeneous worlds.

But what is the exact role of ligands? They initially serve as capping agents to limit the growth and maintain well-dispersed small-size metal NPs and can modify shapes themselves,[9,10] which in turn impacts their catalytic performance.[11–13] More importantly, such a ligand–metal interface is actually quite dynamic and can potentially (i) open or block catalytic sites on the surface, (ii) alter the exposed metal surface, (iii) change the electronic structure of the metal, (iv) impose stereo-electronic effects on reactants and products, and (v) tune properties on the metal/ligand/solvent boundaries.[14] By analogy with the sergeants-and-soldiers principle,[15,16] its role may be described as a cooperative action of small individuals that contributes to amplify a certain chemical property, such as activity, selectivity, or stability.

The concept of surface functionalization is not new; rather, it was commonly referred to as molecular modifiers doing poisoning or passivation of unselective sites. A textbook example is the Lindlar catalyst for the selective hydrogenation of alkynes to alkenes,[17,18] where Pd NPs supported on $CaCO_3$ are modified with lead and quinoline to modulate hydrogen coverage, alkyne adsorption, alkene desorption, and the size of active Pd ensembles.[19]

The purpose and fate of ligands in nanocatalysts have been reviewed in recent years, mostly trying to unravel their impact at structural level.[8,20–33] However, detailed information on the operating mechanisms of these complex systems is still scarce[34] and this hampers a steady innovation in the field. Here is where density functional theory (DFT) simulations come into play to provide insight into catalytic processes at the atomic scale,[35–37] particularly since the methods to study molecular and periodic systems are now robust enough to maintain a common framework for both homogeneous- and heterogeneous-like contributions. In this mini-review, we will analyse recent first-principles studies of reaction mechanisms promoted by decorated metal NPs, with

Institute of Chemical Research of Catalonia (ICIQ), Barcelona Institute of Science and Technology (BIST), Av. Països Catalans 16, 43007 Tarragona, Spain.
E-mail: mortuno@iciq.es, nlopez@iciq.es

special emphasis on the role of ligands in controlling activity and selectivity. As discussed below, it would soon become clear that the main computational challenges concern the huge system size and the dynamic features intrinsically associated with it. In this line, using open-access platforms to store and share computational results, such as ioChem-BD[38] or Catalysis Hub,[39] is crucial for reproducibility and data mining[40] of metal–ligand interfaces.

Challenges of metal–ligand interface simulations

The first hurdle when employing DFT to describe metal NPs relates to its size. For diameters larger than 2 nm, the so-called scalable regime, NPs are represented by infinite surfaces.[41] This approach is not always possible and particularly in the very small regime, *ca.* 1 nm diameter or less, the optimization of the nanostructured system constitutes a better approach as extensively reported for Au nanoclusters.[42,43] In addition, ligands at the interface may be relatively large[44] for which several configurations need to be thoroughly sampled as they cover the surface with very dense concentrations.

Another challenge when modelling interfaces is that the metal NP is better represented as a solid with continuous bands, while typical organic ligands are finite in size and characterised by molecular orbitals and the interactions have a large contribution from van der Waals forces.[45,46] In those cases where the ligands have formal charges, such as surfactants or ionic liquids, the description of different types of bonds (covalent *vs.* ionic *vs.* dispersion) needs to be carefully balanced. For solvent average contributions, they may be taken into account either explicitly or implicitly, but again a detailed balance of all bonding contributions is required.[47,48]

Finally, for detailed modelling of solvents and ionic liquids, the dynamic behaviour of the layer constitutes a major issue. Thus, the study of complex reactivity in these highly computationally demanding interfaces is at the frontier of theoretical simulations.

The mini-review is structured according to the nature of the species at the interface with the metal catalyst: molecular organic ligands, surfactants, and ionic liquids (Fig. 1). We then follow up with a brief section on deactivation pathways. Overall, understanding the concepts behind each system at the atomic scale might lead to the generation of unified theories for future catalyst design.

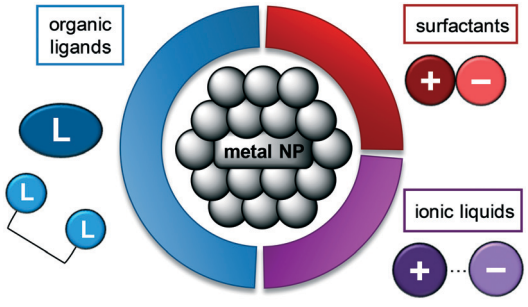

Fig. 1 Ligand–metal interfaces reviewed herein.

2. Organic ligands

This section collects computational mechanistic contributions on metal NPs and surfaces coated with organic ligands regardless of their origin: as-synthesised, post-synthetic exchange, added during catalysis, *etc.*

C-based ligands

N-heterocyclic carbenes (NHCs)[49] are versatile ligands not only for transition metal molecular catalysts but also for surfaces and materials.[50,51] Recent combined experiment–theory studies are devoted to structural features and binding modes of NHCs on NPs[52,53] and surfaces[54–56] but detailed investigations on reaction mechanisms are less common.

Muratsugu, Doltsinis, Glorius, and co-workers reported the synthesis of NHC-decorated Pd NPs for the hydrogenolysis of bromobenzene.[57] The C–Br bond breaking process was computed at DFT level using clean and modified Pd_{13} clusters. Smaller energy barriers were estimated for NHC-decorated clusters bearing aromatic groups (<0.10 eV); *cf.* those involving alkyl moieties (0.13 eV) and the clean catalyst (0.17 eV). Such a trend did correlate with computed ionization potentials, which highlighted the electronic effects of these strong σ-donating ligands. In other words, considerations and knowledge from traditional descriptors in organic chemistry can be successfully transferred to decorated metal NPs.

Wen, Copéret, Chang, and co-workers supported a chelating NHC on Pd electrodes for electrochemical CO_2 reduction (CO_2RR) to formate and CO.[58] Compared to clean surfaces, the NHC-decorated Pd system generated a significant amount of formate. To rationalise these results, they performed DFT calculations on clean and NHC-decorated Pd(111) surfaces with adsorbed H atoms to estimate activation energies (Scheme 1). The modified surface systematically provided lower Gibbs energy barriers for the first and second hydrogen transfers to yield formic acid. The same trend was observed

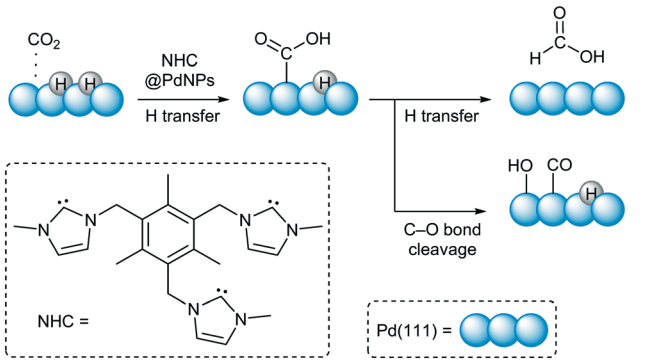

Scheme 1 Electrochemical CO_2 reduction catalysed by NHC-decorated Pd(111) surfaces.

for the C–O bond cleavage to form CO, which further explained the selectivity experimentally observed.

The reactants themselves can also modify the mechanism. A clear example is the semi-hydrogenation of propyne on Ag surfaces reported by Vilé *et al.* (Scheme 2).[59] DFT simulations predict an endothermic H–H bond breaking process on Ag(211) with a large energy barrier of 1.33 eV. However, the coordination of propyne on a stepped Ag(211) induces a metastable intermediate that promotes an exothermic and heterolytic H_2 activation process with a lower barrier of 1.03 eV. This implies that surface decoration can take place even from reactants.

N-based ligands

The use of chiral ligands, particularly amines and alkaloids, has been widely exploited to promote enantioselective transformations in surface catalysis.[60] Pioneering studies by Baiker and co-workers extensively studied metal-catalysed enantioselective hydrogenations induced by cinchona alkaloids as surface modifiers (Scheme 3).[61] They employed computational approaches to identify the active centre *pockets* responsible for chirality transfer from the metal–alkaloid interface to the products.[62,63] Nevertheless, the adsorption mode of some aromatic amines is still under debate.[64,65]

Kunz and co-workers explored the asymmetric hydrogenation of keto esters catalysed by Pt NPs decorated with amino acids.[66] Computational studies described the adsorption of alanine on Pt(111) *via* the N atom and proposed different binding modes between the reactant methyl acetoacetate and the ligand moiety to account for the chirality transfer.[67]

N-containing compounds can also play an important role in hydrogenation reactions *via* the so-called frustrated Lewis pair (FLP) activity.[68] FLP-type mechanisms in heterogeneous catalysis[69] typically involve the organic ligand as a Lewis base and the metal surface as a Lewis acid. Such approach is commonly employed in Au-based catalysts[70] to overcome their inertness towards H_2 activation.[71]

Guo and co-workers firstly reported a computational study on the heterolytic splitting of dihydrogen on Au(111) using small N-based compounds as probe Lewis bases.[72] While the clean Au surface breaks the H–H bond in a homolytic way demanding 1.20 eV (Scheme 4a), the lone pair of ammonia promotes a heterolytic cleavage *via* 0.65 eV (Scheme 4b). When using the more sterically demanding 2-propanimine ligand, the energy barrier further decreases to 0.43 eV. However, the lack of bond between the N and the surface would impose severe entropic penalties to these transition states.

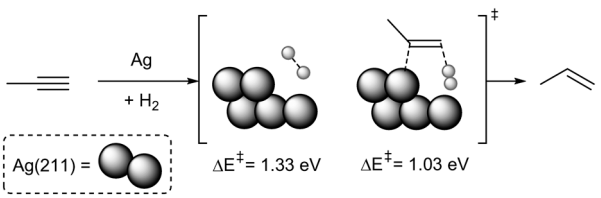

Scheme 2 Homolytic and alkyne-promoted heterolytic H–H bond activations on Ag(211) surfaces.

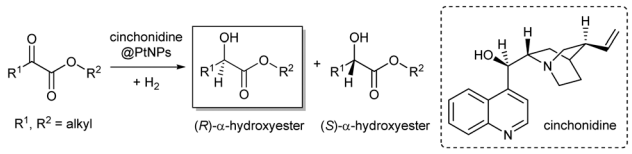

Scheme 3 Enantioselective hydrogenation of α-keto esters catalysed by alkaloid-decorated Pt NPs.

Later, Rossi and co-workers reported the Au-catalysed semi-hydrogenation of alkynes using amines as additives[73] or grafted ligands.[74] DFT simulations confirmed the role of different amines in promoting the heterolytic H_2 dissociation. In contrast to the high activation barriers and endothermicity associated with clean Au surfaces, the piperazine-capped system cleaves the H–H bond with an activation barrier of 0.32 eV, forming a thermoneutral product. The reaction continues with subsequent hydride and proton transfers to yield the corresponding alkene. From these results, theory predicted a linear correlation between H–H bond activation energies for bidentate ligands and experimental reaction rates (Fig. 2a), thus identifying for the first time a descriptor for the ligand directly from the computational results.[73] Similar trends were found for processes assisted by 1,10-phenanthroline (Fig. 2b).[74]

Shi and co-workers reported the synthesis of DMF from dimethylamine and CO_2/H_2 using Cu catalysts.[75] One major issue of this process is further hydrogenation of the product DMF to trimethylamine. However, they managed to control the selectivity by adding 1,10-phenanthroline. According to DFT studies, they claimed that C–H bond forming and C–O bond breaking reactions *via* decorated Cu(111) required higher energy barriers than those *via* clean metal, which explains the higher selectivity experimentally observed.

Poteau and co-workers computed the interaction of Ru_{55} NPs[76] with aminidates for hydrogenation processes[77] and 4-phenylpyridine for the hydrogen evolution reaction (HER).[78] Atomistic information about the role of the ligands in the operating mechanisms is not available yet.

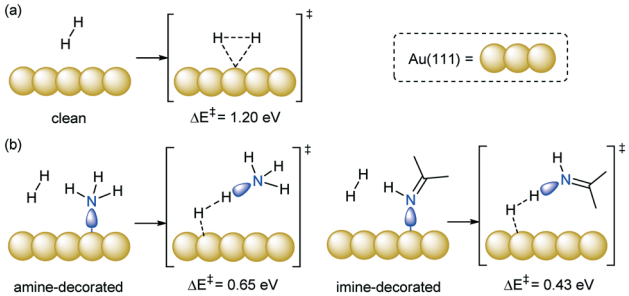

Scheme 4 Homolytic (a) and N-promoted heterolytic (b) H–H bond activations on Au(111) surfaces.

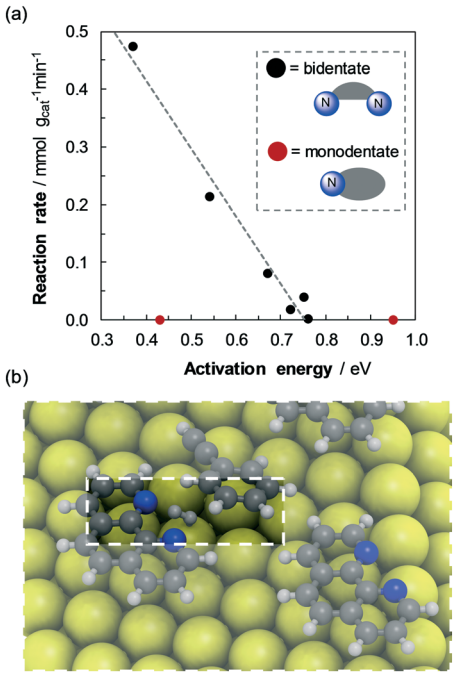

Fig. 2 Linear correlation between computed activation energies and experimental reaction rates (a) and transition state structure for the heterolytic H–H bond activation *via* 1,10-phenanthroline on Au(111) surfaces (b).

P-based ligands

Phosphine compounds are common ligands in homogeneous catalysis due to their fine-tuning properties.[79] In the heterogeneous world, phosphines are usually employed as NP stabilisers, but their tunability for catalytic performance is attracting great interest.[80]

Lambert and co-workers first reported the use of ligand-stabilised Au NPs, $[Au_{55}(Ph_3P)_{12}Cl_6]$, as selective catalysts for styrene oxidation by dioxygen.[81] Benzaldehyde was the major product of the reaction, followed by styrene epoxide and acetophenone. Based on these experimental findings, Zeng and co-workers performed a DFT study on these ligand-decorated Au_{55} NPs (Scheme 5).[82] They thoroughly explored the configurational space of Au nanoclusters and identified Au_6 faces, so-called triangle sockets, as the reactive sites. The initial O_2 dissociation[83] at clean Au_{55} clusters was unlikely, presenting an energy barrier of 1.95 eV and a reaction energy of 0.97 eV. In contrast, the PPh_3-decorated Au_6 face allowed a two-step process *via* a superoxo-like intermediate with an overall energy barrier of 1.22 eV and a reaction energy of 0.45 eV. Further calculations demonstrated that the ligands not only stabilise the cluster but also impact the electronic structure of the gold core, promoting O_2 activation.[84] After O_2 dissociation, they computed the reaction mechanisms of styrene oxidation to account for all observed products.[82] While the formation of styrene oxide and acetophenone required 1.08 and 1.16 eV, respectively, the confinement of ligands around the active site favoured the pathway towards benzaldehyde with a lower energy barrier of 0.86 eV.

van Leeuwen and co-workers employed secondary phosphine oxide (SPO) ligands[85] to prepare gold catalysts for the selective hydrogenation of α,β-unsaturated aldehydes.[86] In particular, SPO-stabilised Au NPs catalysed the hydrogenation of acrolein to allyl alcohol (Scheme 6), even though the hydrogenation of C=C bonds is thermodynamically favoured. To rationalise the experimental product distribution, López and co-workers modelled a Au_{55} NP decorated with 27 Ph_2PO ligands.[87] The H_2 dissociation on clean Au_{55} presented an energy barrier of 0.78 eV and an endothermic reaction energy of 0.10 eV. The decorated NP, however, exhibited a lower energy barrier of 0.54 eV with an exothermic reaction energy of 0.64 eV. Such a sharp difference comes from the organic ligand which actively participates in the reaction by promoting a concerted transfer hydrogenation mechanism. Similar to the previously discussed FLPs, the lone pair of the oxygen

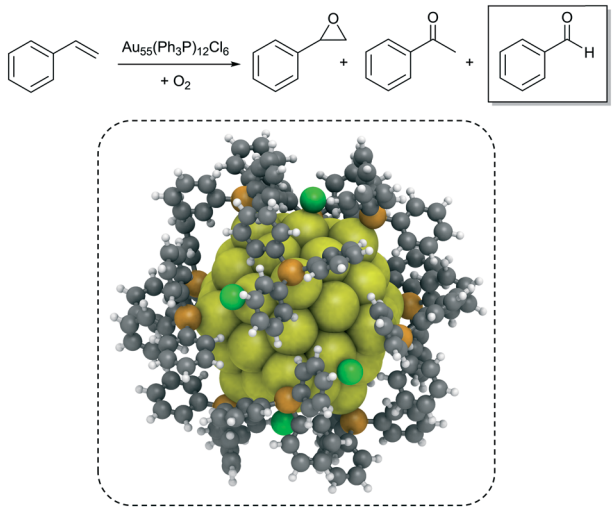

Scheme 5 Oxidation of styrene catalysed by phosphine-decorated Au_{55} NPs (Au = yellow, Cl = green, P = orange, C = grey, H = white).

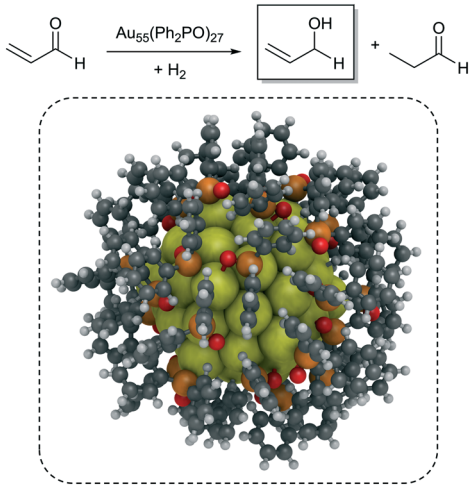

Scheme 6 Hydrogenation of acrolein catalysed by SPO-decorated Au_{55} NPs (Au = yellow, P = orange, O = red, C = grey, H = white).

abstracts one H atom as a proton while the other H atom is adsorbed on the metal surface as a hydride. Such a charge-separation feature favoured the selective hydrogenation of the more polar C═O moiety, compared to the C═C bond, by 0.08 eV. Finally, the authors built a multidimensional linear scaling relationship using a two-variable descriptor based on the electronic (the energy difference between the HOMO of the ligand and the HOMO of the substrate) and geometric effects (the empty sites on the NP surface obtained from experimental NP sizes and metal : ligand ratios).

For metal catalysts where H_2 activation is not rate-determining, such as Pd and Pt, steric effects become more relevant. Honkala and co-workers found that the selectivity of acrolein hydrogenation on Pd(111) and Pt(111) is controlled by the concentration of the reactant at the surface, where high coverage favours C═C bond hydrogenation.[88]

Chatterjee and Jensen reported the synthesis of Pd NPs capped with phosphine ligands to catalyse the deoxygenation of fatty acids to alkenes *via* anhydride intermediates (Scheme 7).[89,90] While the PPh_3-modified Pd catalyst performed poorly, the use of bidentate Xantphos-like ligands,[91] such as DPEphos, resulted in good yields and excellent selectivity towards terminal alkenes.[89] Inspired by these results, we computationally addressed the deoxygenation of pentanoic anhydride as a model substrate on phosphine-decorated Pd(111) surfaces to unravel the underlying reaction pathway.[92] We observed that monodentate PPh_3 ligands fully cover the Pd surface, forming a self-assembled monolayer, which poisons the NP surface and prevents the approach of the substrate (Fig. 3a). On the other hand, the chelating effect of bidentate phosphines created a transient cavity on the surface (Fig. 3b) which was able to capture the reactant (adsorption energy of −0.62 eV) and promote the deoxygenation reaction (activation energy of 1.19 eV). Moreover, the steric hindrance imposed by the ligands at the catalytic site prompted the release of terminal alkene products, thus precluding their further isomerization into internal derivatives. The displacement of adsorbed alkenes by ligands has also been suggested to prevent over-hydrogenation of alkynes on Cu NPs.[93] In this case, thermodynamic selectivity, *i.e.* the ranking of adsorption energies between all the species involved, turns out to be an easy yet practical descriptor.[94]

S-based ligands

Due to the particular properties of the Au–S interface,[95,96] thiol ligands have been extensively used to stabilise atomically precise Au nanoclusters.[97–101] The literature on this field

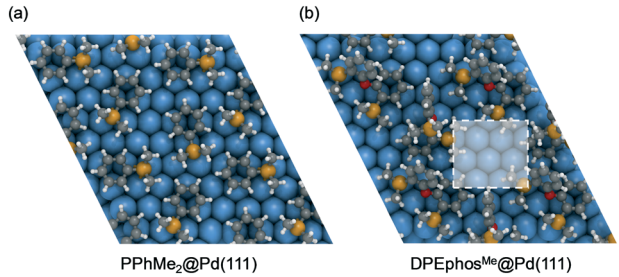

Fig. 3 Steric environment imposed by monodentate (a) and bidentate (b) phosphines on Pd(111) surfaces. The cavity is highlighted with a white square (Pd = light blue, P = orange, O = red, C = grey, H = white).

is vast[102] and computational studies on structural and electronic features can be found elsewhere.[42,43,95,103–109] Instead, we will focus on recent theoretical contributions that directly address reaction mechanisms.

Jin and co-workers reported a selective CO_2RR to CO using thiolate-capped Au_{25} clusters.[110] Following that study, Kauffman and co-workers computed the electrochemical pathway using $Au_{25}(SCH_3)_{18}$ models.[111,112] They found an onset potential of −2.04 V for the formation of adsorbed COOH,[112] which dramatically differed from the experimental value of −0.19 V (*vs.* reversible hydrogen electrode).[110] The removal of one ligand created an accessible catalytic site to stabilise the key COOH intermediate (Scheme 8), which led to an onset potential of −0.34 V, much in line with experiments.

Mpourmpakis and co-workers computationally proved the relevance of ligand removal to understand CO_2RR trends for different Au_{25} morphologies.[113] They performed a systematic comparison between CO_2RR and HER on $Au_{25}(SCH_3)_{18}$ and $Au_{25}(SCH_3)_{17}$ for several charge states.[114] They found that H_2 formation is favoured for all systems but $Au_{25}(SCH_3)_{17}^-$, which would be selective towards CO_2 reduction by 0.28 eV. In the same line, Kauffman and co-workers reported that Cu–S interfaces at mixed Cu/Au NPs stabilised the binding of CO with respect to that of H, thus enhancing selectivity.[115] However, the release of ligands would hamper the reaction *via* irreversible CO adsorption.

Continuing with electrochemical processes, Lee, Jiang, and co-workers reported mono-atom-doped Au clusters for efficient HER.[116,117] First-principles studies indicated that the H atom behaves as a metal in $[H\text{-}M_1\text{-}Au_{24}(SR)_{18}]$ species, in

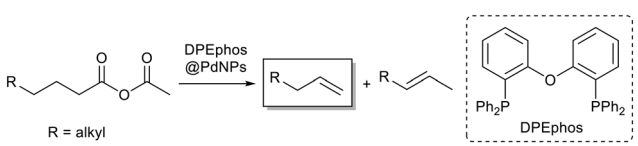

Scheme 7 Decarbonylation of anhydrides catalysed by phosphine-decorated Pd NPs.

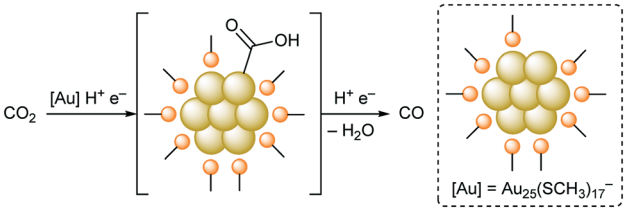

Scheme 8 Electrochemical CO_2 reduction to CO catalysed by thiolate-decorated Au_{25} nanoclusters.

contrast to their hydride or electron-withdrawing role found in phosphine-capped derivatives.[118]

Jin and co-workers reported the selective hydrogenation of α,β-unsaturated ketones and aldehydes to alcohols catalysed by $Au_{25}(SR)_{18}$ nanoclusters.[119] Jiang and co-workers explored several reaction pathways to explain these experimental results.[120] Since dissociation of H_2 on $Au_{25}(SCH_3)_{18}$ involved an energy barrier of >2 eV, they proposed H_2 splitting assisted by the substrate. For all computed mechanisms, the H–H bond activation process occurred *via* hydride transfer to the Au nanocluster and proton transfer to the C=O and C=C groups of the substrate (Scheme 9). The lower activation energy found for C=O (0.99 eV) *cf.* C=C (1.12 eV) was attributed to the different polarity of the bonds. The explicit inclusion of ethanol solvent molecules as proton shuttles did not significantly impact the C=O hydrogenation barrier (0.94 eV).

Jin and co-workers performed the Ullmann C–C coupling reaction between two different iodobenzenes using $Au_{25}(SR)_{18}$ and found that selectivity towards the heterocoupling product was substantially increased with aryl thiolates compared to alkyl derivatives.[121] After removal of one ligand to create a vacant site, DFT predicts isoenergetic transition states for hetero- and homocoupling products for S-methyl, while the transition state leading to the hetero-coupling product is energetically favoured by 0.12 eV for S-naphthyl.

Zheng, Häkkinen, and co-workers reported the hydrogenation of ketones to alcohols under mild conditions catalysed by thiolate-protected $Cu_{25}H_{10}$ nanoclusters (Scheme 10).[122] DFT indicates that neither H_2 nor formaldehyde can initially bind to the cluster. Instead, one hydride from the catalyst is transferred to the C atom of C=O while the O atom binds to Cu. After that, the reaction continues *via* two competitive pathways: (i) heterolytic H_2 splitting at the Cu–O interface or (ii) second transfer followed by H_2 dissociation on the metal cluster.

Wen, Liu, and co-workers capped Au NPs with S-based tetradentate porphyrin ligands for electrocatalytic CO_2RR.[123] DFT calculations resulted in a large stabilisation energy of 0.55 eV for the COOH intermediate when comparing ligand-modified *vs.* clean Au(111) surfaces.

Flake, Xu, and co-workers computed HER and CO_2RR intermediates on Au(211) facets capped with 2-phenylethanethiol (PET) and 2-mercaptopropanoic acid (MPA), where the former showed a better performance for CO_2RR.[124] On the

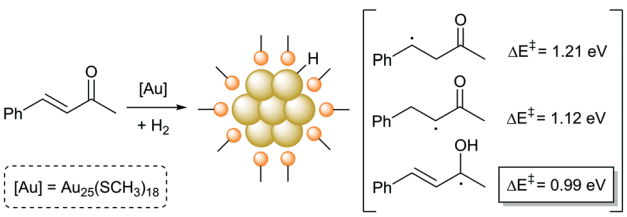

Scheme 9 Hydrogenation of α,β-unsaturated ketones catalysed by thiolate-decorated Au_{25} nanoclusters.

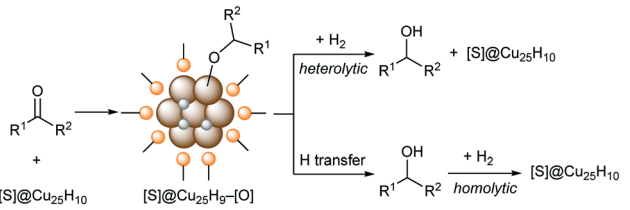

Scheme 10 Hydrogenation of carbonyl groups catalysed by thiolate-decorated $Cu_{25}H_{10}$ nanoclusters.

one hand, PET ligands created local negative dipole moments that stabilised adsorbed COOH species. On the other hand, MPA ligands extended over the surface and clashed with adsorbed H and COOH intermediates.

Moving away from Au, thiols were also employed to coat the surface of other metal NPs.[125,126] Janik, Medlin, and co-workers reported the effect of alkanethiol-modified Pd catalysts for the selective hydrogenation of furfuryl alcohol to methylfuran (Scheme 11a).[127] DFT studies suggested that conversion of furfural alcohol to either methylfuran *via* hydrodeoxygenation (HDO) or furan *via* decarbonylation (DC) are comparable for clean Pd(111) and Pd(221) surfaces. On the contrary, methanethiol-coated Pd(221) surfaces created a confined environment that induces the vertical adsorption of the substrate and precluded the co-adsorption of DC intermediates, thus increasing the selectivity towards methylfuran *via* HDO (Scheme 11b). Similar flat and tilted configurations were reported by Vlachos and co-workers as a function of furfural coverage.[128]

Other ligands

Neurock, Tysoe, and co-workers studied the formation of vinyl acetate on Pd(111) at low and high coverage situations.[129] Following a Samanos-type mechanism, an adsorbed acetate reacted with ethylene forming an acetoxyethyl intermediate which then underwent β-H elimination (Scheme 12). DFT studies predicted a significantly lower energy barrier for the C–O coupling at high acetate coverage. Such a trend was explained as a competition between neighbouring acetate groups, which decreased their nucleophilicity and thus enhanced their reactivity towards ethylene. Similarly, a realistic simulation of formate coverage provided reaction rates in line

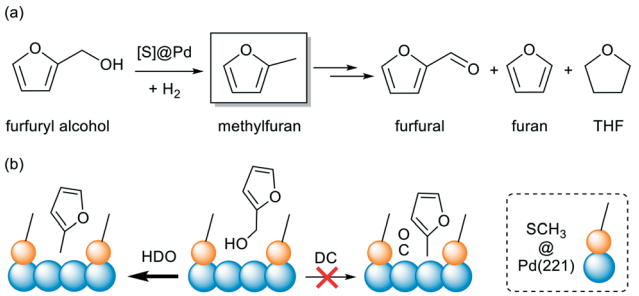

Scheme 11 Hydrogenation of furfuryl alcohol catalysed by thiolate-decorated Pd NPs (a) and reaction mechanisms imposed by coverage (b).

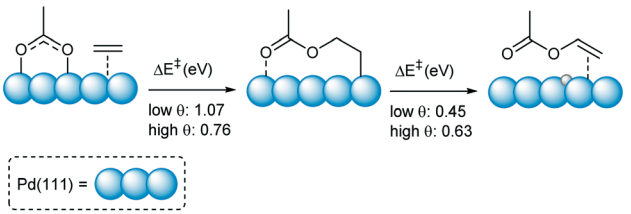

Scheme 12 Synthesis of vinyl acetate catalysed by acetate-decorated Pd(111) surfaces.

with experiments for Cu-catalysed CO_2 hydrogenation to methanol.[130] Poteau, Philippot, and co-workers predicted a promising HER catalyst based on acetate-capped Ru NPs.[131]

Wang and co-workers modified Cu electrodes with amino acids to enhance the selectivity of electrochemical CO_2RR towards hydrocarbons, where glycine performed best in terms of faradaic efficiency.[132] They computed the free energy change of CO_2 and CO protonation for clean and zwitterionic-glycine-decorated Cu(110) surfaces. DFT studies showed that the NH_3^+ group from glycine stabilised adsorbed COOH and CHO intermediates *via* H-bond-like interactions by *ca.* 0.5 and 0.2 eV, respectively, with respect to the clean surface.

Saeys and co-workers computed the reaction mechanism of catalytic transfer hydrogenation of ketones on Cu(111).[133] Using a coverage-dependent microkinetic model, they demonstrated a direct proton transfer between the sacrificial alcohol and the ketone, which avoids surface-bound hydride intermediates.

Knecht, Naik, Heinz, and co-workers reported Stille cross-coupling reactions catalysed by peptide-capped Pd NPs,[134–136] where the catalytic activity was estimated by computing the energy associated with the rate-determining leaching of one Pd atom from the bulk NP.[137] In analogy to peptides, organic polymers can also coat metal surfaces and have an impact in catalysis. However, these systems are beyond the scope of the current work.

3. Surfactants

Surfactants may behave differently from typical organic ligands as they are constituted by close contact ion pairs, involving ionic and van der Waals interactions with the metal. One of the most successful systems involving surfactants is the so-called NanoSelect™ patented by BASF.[138] The water-soluble hexadecyl(2-hydroxyethyl)dimethylammonium dihydrogenphosphate (HHDMA, Fig. 4a) is employed to prepare Pd catalysts for the hydrogenation of terminal alkynes to alkenes, surpassing Pb-free Lindlar systems.[139,140] To fully understand the performance of NanoSelect™, the structure of such hybrid catalysts should be first characterised. In that sense, atomistic simulations were carried out at the interface between HHDMA and Pd(111).[141,142] DFT results showed that the anion binds to Pd, which might involve O–H dissociation, while the cation stays close to the anion by electrostatic and H-bond interactions. At low concentration of HHDMA, the aliphatic chain lies flat on the metal surface. With increasing ligand loadings, it moves upwards and forms a monolayer that coats the NP (Fig. 4b). Classical molecular dynamics (MD) simulations indicated that such long chains are highly mobile and can adapt the approach of substrate molecules to the surface under catalytic conditions.

Pérez-Ramírez and co-workers employed NanoSelect™ for the selective direct synthesis of hydrogen peroxide (Scheme 13).[143] The reaction mechanisms for clean and HHDMA-decorated Pd(111) surfaces were computed at DFT level. The mechanism starts with O_2 adsorption on the catalyst surface followed by hydrogenation *via* hydroperoxy OOH intermediates. Although the activation energy to form H_2O_2 is lower for the clean surface (0.74 eV) than that for the modified catalyst (1.18 eV), side reactions are faster for the former. Indeed, the environment imposed by the surfactant–metal interface induces a vertical adsorption of O_2 and OOH intermediates (Scheme 13), *i.e.* a conformational change that precludes alternative pathways involving O–O bond cleavages and, therefore, increases selectivity.

Pt-based NanoSelect™ catalysts have also been used for the hydrogenation of nitroarenes to anilines.[144–147] Haber-type mechanisms were computed for Pb-modified Pt(111) as well as clean Pt(111),[146] where nitrobenzene was adsorbed in a vertical way to mimic the environment imposed by the surfactant. Further DFT simulations using a fully atomistic model of decorated Pt NPs (Fig. 5a)[147] showed that the ion pairs can induce a local electrostatic field[148,149] at the surfactant–metal interface, which promoted an electrochemical-like effect with heterolytic H_2 splitting in the presence of water (Fig. 5b), as well as the formation of high-energy electrons confined in the metal. These electrons can then be effectively transferred to the nitrobenzene, increasing the adsorption and thus the reactivity.

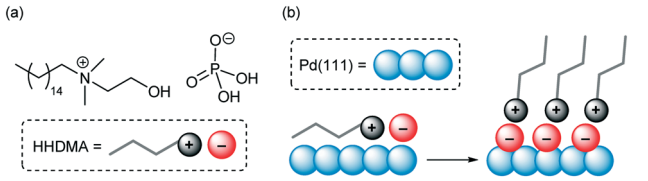

Fig. 4 Structure of HHDMA (a) and its coordination modes on Pd(111) surfaces (b).

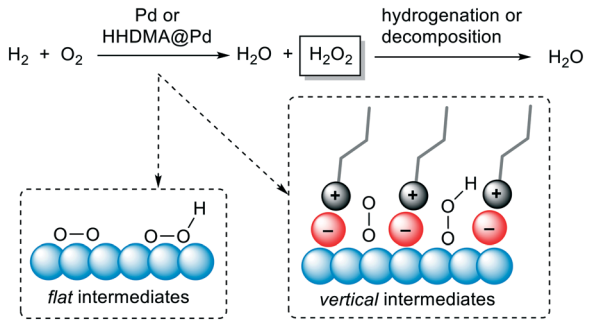

Scheme 13 Direct synthesis of hydrogen peroxide catalysed by clean and HHDMA-decorated Pd NPs.

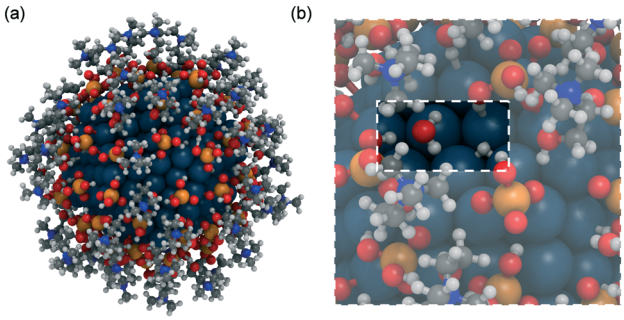

Fig. 5 Surfactant-decorated Pt_{260} nanoparticle (a) and closer look at the electrochemical interface (b) (Pt = dark blue, P = orange, O = red, N = blue, C = grey, H = white).

In the same line, HHDMA-decorated Ru NPs have been employed for the hydrogenation of levulinic acid to γ-valerolactone (Scheme 14).[150] The complete reaction network was explored for a clean Ru(0001) surface, while only the most relevant steps were considered for the HHDMA-decorated Ru(0001) model. DFT calculations predicted a barrierless H_2 dissociation on the surface, followed by C–OH cleavage, ring closing, and hydrogenation steps. The key role of the surfactant relies on its ability to locally make the metal–ligand–water interface more acidic, thus opening faster reaction pathways compared to those for the clean surface.

4. Ionic liquids

Ionic liquids (ILs) are widely employed as stabilising agents of metal NPs during their synthesis[151] and catalytic applications.[152] Contrary to the previously discussed ligands, where different coverages may be considered, ILs should be described as a condensed phase to properly account for their electrostatic and dynamic properties.[153] Otherwise, cluster models[154] would not account for the effect of the bulk liquid and continuum methods[155] would fall short to describe key solute–solvent interactions. In such a situation, the computational modelling of metal–IL interfaces is mainly dominated by force-field-based MD simulations; see for instance the IL solvation of metal surfaces[156,157] and metal NPs.[158–160] The role of ILs on non-metal surfaces has also been studied, such as shifts in TiO_2 band levels[161] and interactions at the interface with sapphire[162] and graphite.[163] Despite the valuable structural information that can be obtained from classical MD, *ab initio* simulations are required to properly describe bond-breaking and bond-forming processes during chemical transformations.

Lawson and co-workers studied the decomposition of ILs at the interface with Li(100) by means of *ab initio* MD.[164] For [C_4C_1pyrr][TFSI] (Chart 1), they observed that only anions decompose, and the resulting F and O atoms penetrate the Li layers. On the other hand, [EMIM][BF_4] (Chart 1) was stable.

Fenter and co-workers reported the reconstruction of Bi electrodes in alkyl-imidazolium-based ILs under CO_2RR conditions. Interestingly, such behaviour was not observed when using electrolytes containing tetrabutylammonium (TBA).[165] A combined experiment–theory effort later explained the origin of such a phenomenon.[166] The authors performed reactive MD simulations with a three-component model consisting of graphene, Bi(001), and cationic species [BMIM] (Chart 1) and TBA. In line with experiments, they observed that [BMIM] cations bind more strongly and induce a higher degree of distortion to the charged Bi(001) slab than TBA. Additional DFT calculations in smaller systems confirmed the previous adsorption energy trends and predicted the partial dissolution of Bi at negative potentials.

MacFarlane and co-workers reported high selectivity for electrochemical nitrogen reduction reaction (NRR) over HER using metal NPs and fluorinated ILs.[167,168] Later, Ortuño *et al.* modelled a metal–IL interface using [C_4C_1pyrr][FAP] (Chart 1) to understand the origin of such selectivity.[169] First, they built a bulk IL phase on a Ru(0001) slab. After equilibration with classical and *ab initio* MD, they computed NRR and HER intermediates for clean and IL-modified metal surfaces at DFT level. They found that stabilising interactions between the key intermediate Ru–N_2H and the F atoms of the anions steered the reaction towards ammonia production (Scheme 15).

5. Deactivation pathways

Although sometimes overlooked, considering catalyst stability is crucial for the computational prediction of realistic and feasible systems. Metal stability in multi-metallic materials is typically employed as a filter in high-throughput computational screening of (electro)catalysts.[170] Indeed, such studies also apply to heterometallic metal–ligand interfaces, as recently shown by Taylor and Mpourmpakis,[171] but for such complex systems a few extra criteria need to be taken into

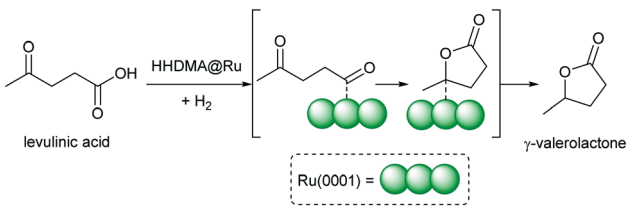

Scheme 14 Hydrogenation of levulinic acid catalysed by HHDMA-decorated Ru(0001) surfaces.

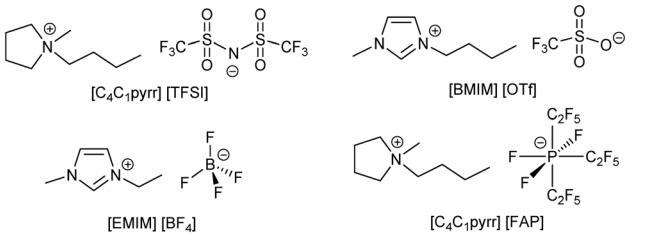

Chart 1 Chemical structures of IL pairs.

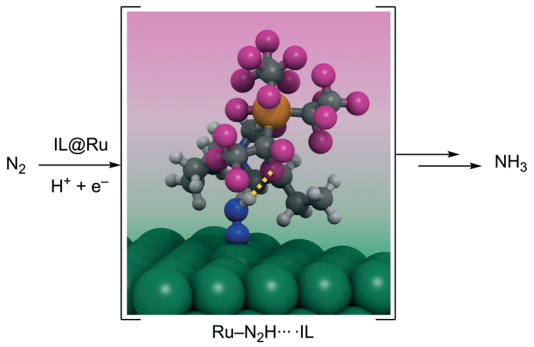

Scheme 15 N_2 reduction catalysed by IL-decorated Ru(0001) surfaces *via* the N_2H intermediate. Only one IL pair is shown for clarity (Ru = dark green, P = orange, F = pink, N = blue, C = grey, H = white).

account, namely: (i) ligand desorption, (ii) ligand degradation, and (iii) ligand-promoted metal leaching.

While strong σ-donating carbenes and phosphines strongly bind to transition metal surfaces, other ligands such as amines may detach under catalytic conditions. A clear example is the amine-assisted FLP H_2 dissociations on Au discussed previously (Scheme 4 and Fig. 2). In those situations, the ligand had to be added in large excess as it was consumed during the catalytic cycle.[73] This problem was later solved by anchoring a N-doped graphene-like layer on top of the catalyst surface.[74]

Regarding ligand stability, phosphine ligands are known to decompose on metal surfaces under thermal treatment. Indeed, such ligand degradation is often exploited as a synthetic protocol to prepare metal phosphides.[172] In this line, recent DFT calculations predicted relatively low energy barriers for the P–C bond breaking process of alkyl phosphines on Ni surfaces.[173] Although these processes usually involve first-row transition metals, ligand decomposition on heavier metals cannot be fully ruled out.[174]

Finally, metal leaching is fairly common in heterogeneous catalysis, but the accurate computation of this process would require the explicit representation of ligands or solvent molecules in the surroundings of the leached species. Heinz and co-workers systematically evaluated abstraction energies of Pd atoms from Pd NPs containing up to 1000 atoms.[137] Zvereva and co-workers found that ILs stabilised Pd clusters through strong polarization interactions,[175] and they further demonstrated that the leaching of Pd atoms can occur *via* ionic [PdX] species rather than *via* "naked" atoms.[176] Catalytic ensembles involving molecular and surface active species are indeed dynamic,[177] and both homogeneous and heterogeneous cycles can co-exist *via* oxidative leaching and deposition processes.[178]

6. Summary and perspectives

Throughout this mini-review we highlighted computational contributions that helped in revealing mechanistic features on ligand-decorated metal NPs in heterogeneous catalysis. There are intrinsic challenges to these interfaces that include: (i) the size of the systems, (ii) the variety of bonds, (iii) the lack of detailed experimental structural knowledge at the interface, and (iv) the dynamic nature of most of the ligands. The ultimate consequence of these limitations is that first-principles reaction mechanisms are still scarce, but the potentiality of bifunctional mechanisms makes them a very attractive research field. Nevertheless, from these pioneering studies we can already see that the combination of a few experimental data and ligand-based descriptors is the faster path forward in the prediction of the properties of complex interfaces and the establishment of robust structure–performance relationships.

As computational catalyst design[179] establishes in heterogeneous[180–182] and homogeneous[183–185] fields, new opportunities arise for systems at the interface between these two worlds. Together with metal–support[186–188] and photo-[189] and electrochemical[190,191] interfaces, the modelling of multicomponent[192] ligand-decorated nanocatalysts has the potential to circumvent typical scaling relationships and thus enhance catalytic performance.

The avenue of new machine learning[193] techniques is rapidly approaching catalysis[194–196] and materials science.[197,198] Chemical descriptors, which typically describe catalytic activity and selectivity, are usually employed as input for algorithms. On the homogeneous side, machine learning protocols have been recently employed to uncover metal–oxo intermediates[199] as well as to screen transition metal catalysts for cross-coupling reactions.[200] On the heterogeneous side, García-Muelas and López demonstrated how principal component analyses and regressions provide adsorption energies on metal surfaces from covalent (d-band center) and ionic (reduction potential) descriptors.[201] Ulissi *et al.* relied on surrogate models to fully explore the syngas reaction network (CO + H_2) on Rh(111).[202] Later, Tran and Ulissi further employed a machine-learning-based workflow to compute 1499 intermetallic materials for CO_2RR and HER.[203] Despite the heavy dependence of these techniques on the descriptors' performance, the combination of electronic structure methods with database repositories and machine learning algorithms seems particularly suited to address the complexity of the catalytic properties of ligand-decorated nanoparticles. We finally point out the importance of interpretability to provide solid scientific meaning to the results obtained from statistical learning models.[204]

Conflicts of interest

There are no conflicts to declare.

Acknowledgements

M. A. O. acknowledges the support of the Beatriu de Pinós postdoctoral programme of the Government of Catalonia's Secretariat for Universities and Research of the Ministry of Economy and Knowledge (2017-BP-00039). M. A. O. and N. L. also acknowledge the Spanish Supercomputing Network

(RES) and the Barcelona Supercomputing Center (BSC) (QCM-2019-1-0030).

References

1 L. Liu and A. Corma, *Chem. Rev.*, 2018, **118**, 4981.
2 D. I. Sharapa, D. E. Doronkin, F. Studt, J.-D. Grunwaldt and S. Behrens, *Adv. Mater.*, 2019, **31**, 1807381.
3 Y. Sun and Y. Xia, *Science*, 2002, **298**, 2176.
4 Y. Xia, Y. Xiong, B. Lim and S. A. Skrabalak, *Angew. Chem., Int. Ed.*, 2009, **48**, 60.
5 H.-G. Liao, D. Zherebetskyy, H. Xin, C. Czarnik, P. Ercius, H. Elmlund, M. Pan, L.-W. Wang and H. Zheng, *Science*, 2014, **345**, 916.
6 M. Grzelczak, J. Pérez-Juste, P. Mulvaney and L.-M. Liz-Marzán, *Chem. Soc. Rev.*, 2008, **37**, 1783.
7 K. An and G. A. Somorjai, *ChemCatChem*, 2012, **4**, 1512.
8 M. A. Boles, D. Ling, T. Hyeon and D. V. Talapin, *Nat. Mater.*, 2016, **15**, 141.
9 G. D. Barmparis, Z. Lodziana, N. López and I. N. Remediakis, *Beilstein J. Nanotechnol.*, 2015, **6**, 361.
10 J. Morales-Vidal, N. López and M. A. Ortuño, *J. Phys. Chem. C*, 2019, **123**, 13758.
11 W. Xu, J. S. Kong, Y.-T. E. Yeh and P. Chen, *Nat. Mater.*, 2008, **7**, 992.
12 Y. Zhang, P. Song, T. Chen, X. Liu, T. Chen, Z. Wu, Y. Wang, J. Xie and W. Xu, *Proc. Natl. Acad. Sci. U. S. A.*, 2018, **115**, 10588.
13 L. Sumner, N. A. Sakthivel, H. Schrock, K. Artyushkova, A. Dass and S. Chakraborty, *J. Phys. Chem. C*, 2018, **122**, 24809.
14 M. Zobel, R. B. Neder and S. A. J. Kimber, *Science*, 2015, **347**, 292.
15 M. M. Green and M. P. Reidy, *J. Am. Chem. Soc.*, 1989, **111**, 6452.
16 L. J. Prins, P. Timmerman and D. N. Reinhoudt, *J. Am. Chem. Soc.*, 2001, **123**, 10153.
17 H. Lindlar, *Helv. Chim. Acta*, 1952, **35**, 446.
18 H. Lindlar and R. Dubuis, *Org. Synth.*, 1973, **5**, 880.
19 M. García-Mota, J. Gómez-Díaz, G. Novell-Leruth, C. Vargas-Fuentes, L. Bellarosa, B. Bridier, J. Pérez-Ramírez and N. López, *Theor. Chem. Acc.*, 2011, **128**, 663.
20 P. Lara, K. Philippot and B. Chaudret, *ChemCatChem*, 2013, **5**, 28.
21 Z. Niu and Y. Li, *Chem. Mater.*, 2014, **26**, 72.
22 S. Campisi, M. Schiavoni, C. E. Chan-Thaw and A. Villa, *Catalysts*, 2016, **6**, 185.
23 C. Amiens, D. Ciuculescu-Pradines and K. Philippot, *Coord. Chem. Rev.*, 2016, **308**, 409.
24 H. Heinz and H. Ramezani-Dakhel, *Chem. Soc. Rev.*, 2016, **45**, 412.
25 S. Kunz, *Top. Catal.*, 2016, **59**, 1671.
26 P. Liu, R. Qin, G. Fu and N. Zheng, *J. Am. Chem. Soc.*, 2017, **139**, 2122.
27 H. Heinz, C. Pramanik, O. Heinz, Y. Ding, R. K. Mishra, D. Marchon, R. J. Flatt, I. Estrela-Lopis, J. Llop, S. Moya and R. F. Ziolo, *Surf. Sci. Rep.*, 2017, **72**, 1.
28 L. M. Martínez-Prieto and B. Chaudret, *Acc. Chem. Res.*, 2018, **51**, 376.
29 L. M. Rossi, J. L. Fiorio, M. A. S. Garcia and C. P. Ferraz, *Dalton Trans.*, 2018, **47**, 5889.
30 J. Yan, B. K. Teo and N. Zheng, *Acc. Chem. Res.*, 2018, **51**, 3084.
31 A. Heuer-Jungemann, N. Feliu, I. Bakaimi, M. Hamaly, A. Alkilany, I. Chakraborty, A. Masood, M. F. Casula, A. Kostopoulou, E. Oh, K. Susumu, M. H. Stewart, I. L. Medintz, E. Stratakis, W. J. Parak and A. G. Kanaras, *Chem. Rev.*, 2019, **119**, 4819.
32 X. Du and R. Jin, *ACS Nano*, 2019, **13**, 7383.
33 W. Wu and E. V. Shevchenko, *J. Nanopart. Res.*, 2018, **20**, 255.
34 S. T. Marshall and J. W. Medlin, *Surf. Sci. Rep.*, 2011, **66**, 173.
35 J. K. Nørskov, F. Abild-Pedersen, F. Studt and T. Bligaard, *Proc. Natl. Acad. Sci. U. S. A.*, 2011, **108**, 937.
36 N. López, N. Almora-Barrios, G. Carchini, P. Blonski, L. Bellarosa, R. García-Muelas, G. Novell-Leruth and M. García-Mota, *Catal. Sci. Technol.*, 2012, **2**, 2405.
37 L. Cusinato, I. del Rosal and R. Poteau, *Dalton Trans.*, 2017, **46**, 378.
38 M. Álvarez-Moreno, C. de Graaf, N. López, F. Maseras, J. M. Poblet and C. Bo, *J. Chem. Inf. Model.*, 2015, **55**, 95.
39 K. Winther, M. J. Hoffmann, O. Mamun, J. R. Boes, J. K. Nørskov, M. Bajdich and T. Bligaard, *Sci. Data*, 2019, **6**, 75.
40 C. Bo, F. Maseras and N. López, *Nat. Catal.*, 2018, **1**, 809.
41 L. Li, A. H. Larsen, N. A. Romero, V. A. Morozov, C. Glinsvad, F. Abild-Pedersen, J. Greeley, K. W. Jacobsen and J. K. Nørskov, *J. Phys. Chem. Lett.*, 2013, **4**, 222.
42 H. Häkkinen, *Chem. Soc. Rev.*, 2008, **37**, 1847.
43 M. Walter, J. Akola, O. Lopez-Acevedo, P. D. Jadzinsky, G. Calero, C. J. Ackerson, R. L. Whetten, H. Grönbeck and H. Häkkinen, *Proc. Natl. Acad. Sci. U. S. A.*, 2008, **105**, 9157.
44 Q. Li and N. López, *ACS Catal.*, 2018, **8**, 4230.
45 S. Grimme, J. Antony, S. Ehrlich and H. Krieg, *J. Chem. Phys.*, 2010, **132**, 154104.
46 N. Almora-Barrios, G. Carchini, P. Błoński and N. López, *J. Chem. Theory Comput.*, 2014, **10**, 5002.
47 K. Mathew, R. Sundararaman, K. Letchworth-Weaver, T. A. Arias and R. G. Hennig, *J. Chem. Phys.*, 2014, **140**, 084106.
48 M. Garcia-Ratés and N. López, *J. Chem. Theory Comput.*, 2016, **12**, 1331.
49 M. N. Hopkinson, C. Richter, M. Schedler and F. Glorius, *Nature*, 2014, **150**, 485.
50 A. V. Zhukhovitskiy, M. J. MacLeod and J. A. Johnson, *Chem. Rev.*, 2015, **115**, 11503.
51 C. A. Smith, M. R. Narouz, P. A. Lummis, I. Singh, A. Nazemi, C.-H. Li and C. M. Crudden, *Chem. Rev.*, 2019, **119**, 4986.
52 M. Rodríguez-Castillo, G. Lugo-Preciado, D. Laurencin, F. Tielens, A. van der Lee, S. Clément, Y. Guari, J. M. López-de-Luzuriaga, M. Monge, F. Remacle and S. Richeter, *Chem. – Eur. J.*, 2016, **22**, 10446.
53 M. R. Narouz, K. M. Osten, P. J. Unsworth, R. W. Y. Man, K. Salorinne, S. Takano, R. Tomihara, S. Kaappa, S. Malola,

C.-T. Dinh, J. D. Padmos, K. Ayoo, P. J. Garrett, M. Nambo, J. H. Horton, E. H. Sargent, H. Häkkinen, T. Tsukuda and C. M. Crudden, *Nat. Chem.*, 2019, **11**, 419.
54 Q. Tang and D.-e. Jiang, *Chem. Mater.*, 2017, **29**, 6908.
55 G. Wang, A. Rühling, S. Amirjalayer, M. Knor, J. B. Ernst, C. Richter, H.-J. Gao, A. Timmer, H.-Y. Gao, N. L. Doltsinis, F. Glorius and H. Fuchs, *Nat. Chem.*, 2017, **9**, 152.
56 A. Bakker, A. Timmer, E. Kolodzeiski, M. Freitag, H. Y. Gao, H. Mönig, S. Amirjalayer, F. Glorius and H. Fuchs, *J. Am. Chem. Soc.*, 2018, **140**, 11889.
57 J. B. Ernst, C. Schwermann, G.-i. Yokota, M. Tada, S. Muratsugu, N. L. Doltsinis and F. Glorius, *J. Am. Chem. Soc.*, 2017, **139**, 9144.
58 Z. Cao, J. S. Derrick, J. Xu, R. Gao, M. Gong, E. M. Nichols, P. T. Smith, X. Liu, X. Wen, C. Copéret and C. J. Chang, *Angew. Chem., Int. Ed.*, 2018, **57**, 4981.
59 G. Vilé, D. Baudouin, I. N. Remediakis, C. Copéret, N. López and J. Pérez-Ramírez, *ChemCatChem*, 2013, **5**, 3750.
60 F. Zaera, *Chem. Soc. Rev.*, 2017, **46**, 7374.
61 T. Bürgi and A. Baiker, *Acc. Chem. Res.*, 2004, **37**, 909.
62 A. Vargas, G. Santarossa, M. Iannuzzi and A. Baiker, *J. Phys. Chem. C*, 2008, **112**, 10200.
63 E. Schmidt, C. Bucher, G. Santarossa, T. Mallat, R. Gilmour and A. Baiker, *J. Catal.*, 2012, **289**, 238.
64 F. Meemken, T. Steiger, M. C. Holland, R. Gilmour, K. Hungerbühler and A. Baiker, *Catal. Sci. Technol.*, 2015, **5**, 705.
65 Y. Ni, A. D. Gordon, F. Tanicala and F. Zaera, *Angew. Chem., Int. Ed.*, 2017, **56**, 7963.
66 I. Schrader, S. Neumann, A. Sulce, F. Schmidt, V. Azov and S. Kunz, *ACS Catal.*, 2017, **7**, 3979.
67 A. Sulce, J. Backenköhler, I. Schrader, M. D. Piane, C. Müller, A. Wark, L. C. Ciacchi, V. Azov and S. Kunz, *Catal. Sci. Technol.*, 2018, **8**, 6062.
68 D. W. Stephan, *Science*, 2016, **354**, aaf7229.
69 Y. Ma, S. Zhang, C.-R. Chang, Z.-Q. Huang, J. C. Ho and Y. Qu, *Chem. Soc. Rev.*, 2018, **47**, 5541.
70 S. Arndt, M. Rudolph and A. S. K. Hashmi, *Gold Bull.*, 2017, **50**, 267.
71 B. Hammer and J. K. Nørskov, *Nature*, 1995, **376**, 238.
72 G. Lu, P. Zhang, D. Sun, L. Wang, K. Zhou, Z.-X. Wang and G.-C. Guo, *Chem. Sci.*, 2014, **5**, 1082.
73 J. L. Fiorio, N. López and L. M. Rossi, *ACS Catal.*, 2017, **7**, 2973.
74 J. L. Fiorio, R. V. Gonçalves, E. Teixeira-Neto, M. A. Ortuño, N. López and L. M. Rossi, *ACS Catal.*, 2018, **8**, 3516.
75 Y. Wu, T. Wang, H. Wang, X. Wang, X. Dai and F. Shi, *Nat. Commun.*, 2019, **10**, 2599.
76 L. Cusinato, L. M. Martínez-Prieto, B. Chaudret, I. del Rosal and R. Poteau, *Nanoscale*, 2016, **8**, 10974.
77 L. M. Martínez-Prieto, I. Cano, A. Márquez, E. A. Baquero, S. Tricard, L. Cusinato, I. del Rosal, R. Poteau, Y. Coppel, K. Philippot, B. Chaudret, J. Cámpora and P. W. N. M. van Leeuwen, *Chem. Sci.*, 2017, **8**, 2931.
78 J. Creus, S. Drouet, S. Suriñach, P. Lecante, V. Collière, R. Poteau, K. Philippot, J. García-Antón and X. Sala, *ACS Catal.*, 2018, **8**, 11094.
79 P. W. N. M. van Leeuwen and J. C. Chadwick, *Homogeneous Catalysts*, Wiley VCH, Weinheim, Germany, 2011, ch. 1.
80 A. J. McCue, F.-M. McKenna and J. A. Anderson, *Catal. Sci. Technol.*, 2015, **5**, 2449.
81 M. Turner, V. B. Golovko, O. P. H. Vaughan, P. Abdulkin, A. Berenguer-Murcia, M. S. Tikhov, B. F. G. Johnson and R. M. Lambert, *Nature*, 2008, **454**, 981.
82 Y. Pei, N. Shao, Y. Gao and X. C. Zeng, *ACS Nano*, 2010, **4**, 2009.
83 M. M. Montemore, M. A. van Spronsen, R. J. Madix and C. M. Friend, *Chem. Rev.*, 2018, **118**, 2816.
84 M. Okumura, Y. Kitagawa, T. Kawakami and M. Haruta, *Chem. Phys. Lett.*, 2008, **459**, 133.
85 E. Rafter, T. Gutmann, F. Löw, G. Buntkowsky, K. Philippot, B. Chaudret and P. W. N. M. van Leeuwen, *Catal. Sci. Technol.*, 2013, **3**, 595.
86 I. Cano, A. M. Chapman, A. Urakawa and P. W. N. M. van Leeuwen, *J. Am. Chem. Soc.*, 2014, **136**, 2520.
87 N. Almora-Barrios, I. Cano, P. W. N. M. van Leeuwen and N. López, *ACS Catal.*, 2017, **7**, 3949.
88 S. Tuokko, P. M. Pihko and K. Honkala, *Angew. Chem., Int. Ed.*, 2016, **55**, 1670.
89 A. Chatterjee and V. R. Jensen, *ACS Catal.*, 2017, **7**, 2543.
90 A. Chatterjee, S. H. H. Eliasson and V. R. Jensen, *Catal. Sci. Technol.*, 2018, **8**, 1487.
91 P. W. N. M. van Leeuwen and P. C. J. Kamer, *Catal. Sci. Technol.*, 2018, **8**, 26.
92 M. A. Ortuño and N. López, *ACS Catal.*, 2018, **8**, 6138.
93 N. Kaeffer, K. Larmier, A. Fedorov and C. Copéret, *J. Catal.*, 2018, **364**, 437.
94 Y. Segura, N. López and J. Pérez-Ramírez, *J. Catal.*, 2007, **247**, 383.
95 H. Häkkinen, *Nat. Chem.*, 2012, **4**, 443.
96 T. Bürgi, *Nanoscale*, 2015, **7**, 15553.
97 P. Maity, S. Xie, M. Yamauchi and T. Tsukuda, *Nanoscale*, 2012, **4**, 4027.
98 G. Li and R. Jin, *Acc. Chem. Res.*, 2013, **46**, 1749.
99 R. Jin, *Nanoscale*, 2015, **7**, 1549.
100 R. R. Nasaruddin, T. Chen, N. Yan and J. Xie, *Coord. Chem. Rev.*, 2018, **368**, 60.
101 T. Higaki, Y. Li, S. Zhao, Q. Li, S. Li, X.-S. Du, S. Yang, J. Chai and R. Jin, *Angew. Chem.*, 2019, **131**, 8377.
102 R. Jin, C. Zeng, M. Zhou and Y. Chen, *Chem. Rev.*, 2016, **116**, 10346.
103 O. Lopez-Acevedo, K. A. Kacprzak, J. Akola and H. Häkkinen, *Nat. Chem.*, 2010, **2**, 329.
104 Y. Pei and X. C. Zeng, *Nanoscale*, 2012, **4**, 4054.
105 D.-e. Jiang, *Nanoscale*, 2013, **5**, 7149.
106 Q. Tang and D.-e. Jiang, *Chem. Mater.*, 2016, **28**, 5976.
107 W. W. Xu, B. Zhu, X. C. Zeng and Y. Gao, *Nat. Commun.*, 2016, **7**, 13574.
108 M. G. Taylor and G. Mpourmpakis, *Nat. Commun.*, 2017, **8**, 15988.
109 Q. Tang, G. Hu, V. Fung and D.-e. Jiang, *Acc. Chem. Res.*, 2018, **51**, 2793.
110 D. R. Kauffman, D. Alfonso, C. Matranga, H. Qian and R. Jin, *J. Am. Chem. Soc.*, 2012, **134**, 10237.

111 D. R. Kauffman, D. Alfonso, C. Matranga, P. Ohodnicki, X. Deng, R. C. Siva, C. Zeng and R. Jin, *Chem. Sci.*, 2014, **5**, 3151.

112 D. Alfonso, D. R. Kauffman and C. Matranga, *J. Chem. Phys.*, 2016, **144**, 184705.

113 S. Zhao, N. Austin, M. Li, Y. Song, S. D. House, S. Bernhard, J. C. Yang, G. Mpourmpakis and R. Jin, *ACS Catal.*, 2018, **8**, 4996.

114 N. Austin, S. Zhao, J. R. McKone, R. Jin and G. Mpourmpakis, *Catal. Sci. Technol.*, 2018, **8**, 3795.

115 D. R. Kauffman, D. Alfonso, D. N. Tafen, C. Wang, Y. Zhou, Y. Yu, J. W. Lekse, X. Deng, V. Espinoza, J. Trindell, O. K. Ranasingha, A. Roy, J.-S. Lee and H. L. Xin, *J. Phys. Chem. C*, 2018, **122**, 27991.

116 K. Kwak, W. Choi, Q. Tang, M. Kim, Y. Lee, D.-e. Jiang and D. Lee, *Nat. Commun.*, 2017, **8**, 14723.

117 G. Hu, Q. Tang, D. Lee, Z. Wu and D.-e. Jiang, *Chem. Mater.*, 2017, **29**, 4840.

118 G. Hu, Z. Wu and D.-e. Jiang, *J. Mater. Chem. A*, 2018, **6**, 7532.

119 Y. Zhu, H. Qian, B. A. Drake and R. Jin, *Angew. Chem., Int. Ed.*, 2010, **49**, 1295.

120 R. Ouyang and D.-e. Jiang, *ACS Catal.*, 2015, **5**, 6624.

121 G. Li, H. Abroshan, C. Liu, S. Zhuo, Z. Li, Y. Xie, H. J. Kim, N. L. Rosi and R. Jin, *ACS Nano*, 2016, **10**, 7998.

122 C. Sun, N. Mammen, S. Kaappa, P. Yuan, G. Deng, C. Zhao, J. Yan, S. Malola, K. Honkala, H. Häkinnen, B. K. Teo and N. Zheng, *ACS Nano*, 2019, **13**, 5975.

123 Z. Cao, S. B. Zacate, X. Sun, J. Liu, E. M. Hale, W. P. Carson, S. B. Tundall, J. Xu, X. Liu, C. Song, J.-h. Luo, M.-J. Cheng, X. Wen and W. Liu, *Angew. Chem., Int. Ed.*, 2018, **57**, 12675.

124 Y. Fang, X. Cheng, J. C. Flake and Y. Xu, *Catal. Sci. Technol.*, 2019, **9**, 2689.

125 J. C. Love, L. A. Estroff, J. K. Kriebel, R. G. Nuzzo and G. M. Whitesides, *Chem. Rev.*, 2005, **105**, 1103.

126 C. A. Schoenbaum, D. K. Schwartz and J. W. Medlin, *Acc. Chem. Res.*, 2014, **47**, 1438.

127 G. Kumar, C.-H. Lien, M. J. Janik and J. W. Medlin, *ACS Catal.*, 2016, **6**, 5086.

128 S. Wang, V. Vorotnikov and D. G. Vlachos, *ACS Catal.*, 2015, **5**, 104.

129 F. Calaza, D. Stacchiola, M. Neurock and W. T. Tysoe, *J. Am. Chem. Soc.*, 2010, **132**, 2202.

130 P. Wu and B. Yang, *ACS Catal.*, 2017, **7**, 7187.

131 R. González-Gómez, L. Cusinato, C. Bijani, Y. Coppel, P. Lecante, C. Amiens, I. del Rosal, K. Philippot and R. Poteau, *Nanoscale*, 2019, **11**, 9392.

132 M. S. Xie, B. Y. Xia, Y. Li, Y. Yan, Y. Yang, Q. Sun, S. H. Chan, A. Fisher and X. Wang, *Energy Environ. Sci.*, 2016, **9**, 1687.

133 J. E. De Vrieze, C. A. Urbina-Blanco, J. W. Thybaut and M. Sayes, *ACS Catal.*, 2019, **9**, 8073.

134 R. Coppage, J. M. Sloick, H. Ramezani-Dakhel, N. M. Bedford, H. Heinz, R. R. Naik and M. R. Knecht, *J. Am. Chem. Soc.*, 2013, **135**, 11048.

135 N. M. Bedford, H. Ramezani-Dakhel, J. M. Sloick, B. D. Briggs, Y. Ren, A. I. Frenkel, V. Petkov, H. Heinz, R. R. Naik and M. R. Knecht, *ACS Nano*, 2015, **9**, 5082.

136 B. D. Briggs, N. M. Bedford, S. Seifert, H. Koerner, H. Ramenazi-Dakhel, H. Heinz, R. R. Naik, A. I. Frenkel and M. R. Knecth, *Chem. Sci.*, 2015, **6**, 6413.

137 H. Ramezani-Dakhel, P. A. Mirau, R. R. Naik, M. R. Knecht and H. Heinz, *Phys. Chem. Chem. Phys.*, 2013, **15**, 5488.

138 P. T. Witte, *WO pat.*, 096783, 2009.

139 P. T. Witte, P. H. Berben, S. Boland, E. H. Boymans, D. Vogt, J. W. Geus and J. G. Donkervoort, *Top. Catal.*, 2012, **55**, 505.

140 P. T. Witte, S. Boland, F. Kirby, R. van Maanen, B. F. Bleeker, D. A. M. de Winter, J. A. Post, J. W. Geus and P. H. Berben, *ChemCatChem*, 2013, **5**, 582.

141 G. Vilé, N. Almora-Barrios, S. Mitchell, N. López and J. Pérez-Ramírez, *Chem. – Eur. J.*, 2014, **20**, 5926.

142 D. Albani, G. Vilé, S. Mitchell, P. T. Witte, N. Almora-Barrios, R. Verel, N. López and J. Pérez-Ramírez, *Catal. Sci. Technol.*, 2016, **6**, 1621.

143 G. M. Lari, B. Puértolas, M. Shahrokhi, N. López and J. Pérez-Ramírez, *Angew. Chem.*, 2017, **129**, 1801.

144 P. Lara and K. Philippot, *Catal. Sci. Technol.*, 2014, **4**, 2445.

145 E. H. Boymans, P. T. Witte and D. Vogt, *Catal. Sci. Technol.*, 2015, **5**, 176.

146 G. Vilé, N. Almora-Barrios, N. López and J. Pérez-Ramírez, *ACS Catal.*, 2015, **5**, 3767.

147 N. Almora-Barrios, G. Vilé, M. Garcia-Ratés, J. Pérez-Ramírez and N. López, *ChemCatChem*, 2017, **9**, 604.

148 S. Shaik, D. Mandal and R. Ramanan, *Nat. Chem.*, 2016, **8**, 1091.

149 A. C. Aragonès, N. L. Haworth, N. Darwish, S. Ciampi, N. J. Bloomfield, G. G. Wallace, I. Diez-Perez and M. L. Coote, *Nature*, 2016, **531**, 88.

150 D. Albani, Q. Li, G. Vilé, S. Mitchell, N. Almora-Barrios, P. T. Witte, N. López and J. Pérez-Ramírez, *Green Chem.*, 2017, **19**, 2361.

151 J. Dupont and J. D. Scholten, *Chem. Soc. Rev.*, 2010, **39**, 1780.

152 J. D. Scholten, B. C. Leal and J. Dupont, *ACS Catal.*, 2012, **2**, 184.

153 B. Kirchner, O. Hollóczki, J. N. Canongia Lopes and A. A. H. Pádua, *WIREs Comput. Mol. Sci.*, 2015, **5**, 202.

154 R. Ludwig, *Phys. Chem. Chem. Phys.*, 2008, **10**, 4333.

155 V. Bernales, A. V. Marenich, R. Contreras, C. J. Cramer and D. G. Truhlar, *J. Phys. Chem. B*, 2012, **116**, 9122.

156 K. C. Jha, H. Liu, M. R. Bockstaller and H. Heinz, *J. Phys. Chem. C*, 2013, **117**, 25969.

157 T. Inagaki, N. Takenaka and M. Nagaoka, *Phys. Chem. Chem. Phys.*, 2018, **20**, 29362.

158 A. S. Pensado and A. A. H. Pádua, *Angew. Chem., Int. Ed.*, 2011, **50**, 8683.

159 A. Podgorsek, A. S. Pensado, C. C. Santini, M. F. Costa Gomes and A. A. H. Pádua, *J. Phys. Chem. C*, 2013, **117**, 3537.

160 F. Fu, Y. Li, Z. Yang, G. Zhou, Y. Huang, Z. Wan, X. Chen, N. Hu, W. Li and L. Huang, *J. Phys. Chem. C*, 2017, **121**, 523.

161 H. Weber and B. Kirchner, *ChemSusChem*, 2016, **9**, 2505.

162 Z. Brkljača, M. Klimczak, Z. Miličević, M. Weisser, N. Taccardi, P. Wasserscheid, D. M. Smith, A. Magerl and A.-S. Smith, *J. Phys. Chem. Lett.*, 2015, **6**, 549.

163 F. Buchner, K. Forster-Tonigold, M. Bozorgchenani, A. Gross and R. J. Behm, *J. Phys. Chem. Lett.*, 2016, **7**, 226.

164 H. Yildirim, J. B. Haskins, C. W. Bauschlicher, Jr. and J. W. Lawson, *J. Phys. Chem. C*, 2017, **121**, 28214.

165 J. Medina-Ramos, S. S. Lee, T. T. Fister, A. A. Hubaud, R. L. Sacci, D. R. Mullins, J. L. DiMeglio, R. C. Pupillo, S. M. Velardo, D. A. Lutterman, J. Rosenthal and P. Fenter, *ACS Catal.*, 2017, **7**, 7285.

166 J. Medina-Ramos, W. Zhang, K. Yoon, P. Bai, A. Chemburkar, W. Tang, A. Atifi, S. S. Lee, T. T. Fister, B. J. Ingram, J. Rosenthal, M. Neurock, A. C. T. van Duin and P. Fenter, *Chem. Mater.*, 2018, **30**, 2362.

167 F. Zhou, L. M. Azofra, M. Ali, M. Kar, A. N. Simonov, C. McDonnell-Worth, C. Sun, X. Zhang and D. R. MacFarlane, *Energy Environ. Sci.*, 2017, **10**, 2516.

168 B. H. R. Suryanto, C. S. M. Kang, D. Wang, C. Xiao, F. Zhou, L. M. Azofra, L. Cavallo, X. Zhang and D. R. MacFarlane, *ACS Energy Lett.*, 2018, **3**, 1219.

169 M. A. Ortuño, O. Hollóczki, B. Kirchner and N. López, *J. Phys. Chem. Lett.*, 2019, **10**, 513.

170 J. Greely, T. F. Jaramillo, J. Bonde, I. Chorkendorff and J. K. Nørskov, *Nat. Mater.*, 2006, **5**, 909.

171 M. G. Taylor and G. Mpourmpakis, *J. Phys. Chem. Lett.*, 2018, **9**, 6773.

172 Y. Pei, Y. Cheng, J. Chen, W. Smith, P. Dong, P. M. Ajayan, M. Ye and J. Shen, *J. Mater. Chem. A*, 2018, **6**, 23220.

173 R. García-Muelas, Q. Li and N. López, *J. Phys. Chem. B*, 2018, **122**, 672.

174 A. M. López-Vinasco, I. Favier, C. Pradel, L. Huerta, I. Guerrero-Ríos, E. Teuma, M. Gómez and E. Martin, *Dalton Trans.*, 2014, **43**, 9038.

175 E. E. Zvereva, S. A. Katsyuba, P. J. Dyson and A. V. Aleksandrov, *J. Phys. Chem. C*, 2016, **120**, 4596.

176 E. E. Zvereva, S. A. Katsyuba, P. J. Dyson and A. V. Aleksandrov, *J. Phys. Chem. Lett.*, 2017, **8**, 3452.

177 D. B. Eremin and V. P. Ananikov, *Coord. Chem. Rev.*, 2017, **346**, 2.

178 J. Jover, M. Garcia-Ratés and N. López, *ACS Catal.*, 2016, **6**, 4135.

179 D. Ess, L. Gagliardi and S. Hammes-Schiffer, *Chem. Rev.*, 2019, **119**, 6507.

180 J. K. Nørskov, T. Bligaard, J. Rossmeisl and C. H. Christensen, *Nat. Chem.*, 2009, **1**, 37.

181 M. M. Montemore and J. W. Medlin, *Catal. Sci. Technol.*, 2014, **4**, 3748.

182 J. Greeley, *Annu. Rev. Chem. Biomol. Eng.*, 2016, **7**, 605.

183 K. N. Houk and H.-Y. Cheong, *Nature*, 2008, **455**, 309.

184 S. Hammes-Schiffer, *Acc. Chem. Res.*, 2017, **50**, 561.

185 C. Poree and F. Schoenebeck, *Acc. Chem. Res.*, 2017, **50**, 605.

186 M.-C. Silaghi, A. Comas-Vives and C. Copéret, *ACS Catal.*, 2016, **6**, 4501.

187 L. Foppa, T. Margossian, S. M. Kim, C. Müller, C. Copéret, K. Larmier and A. Comas-Vives, *J. Am. Chem. Soc.*, 2017, **139**, 17128.

188 T. Whittaker, K. B. S. Kumar, C. Peterson, M. N. Pollock, L. C. Grabow and B. D. Chandler, *J. Am. Chem. Soc.*, 2018, **140**, 16469.

189 F. S. Hegner, D. Cardenas-Morcoso, S. Giménez, N. López and J. R. Galán-Mascarós, *ChemSusChem*, 2017, **10**, 4552.

190 O. M. Magnussen and A. Gross, *J. Am. Chem. Soc.*, 2019, **141**, 4777.

191 J. A. Gauthier, S. Ringe, C. F. Dickens, A. J. Garza, A. T. Bell, M. Head-Gordon, J. K. Nørskov and K. Chan, *ACS Catal.*, 2019, **9**, 920.

192 G. Kumar, E. Nikolla, S. Linic, J. W. Medlin and M. J. Janik, *ACS Catal.*, 2018, **8**, 3202.

193 A. C. Mater and M. L. Coote, *J. Chem. Inf. Model.*, 2019, **59**, 2545.

194 J. R. Kitchin, *Nat. Catal.*, 2018, **1**, 230.

195 B. R. Goldsmith, J. Esterhuizen, J.-X. Liu, C. J. Bartel and C. Sutton, *AIChE J.*, 2018, **64**, 2311.

196 P. Schlexer, K. T. Winther, J. A. Garrido Torres, V. Streibel, M. Zhao, M. Bajdich, F. Abild-Pedersen and T. Bligaard, *ChemCatChem*, 2019, **11**, 1.

197 K. T. Butler, D. W. Davies, H. Cartwright, O. Isayev and A. Walsh, *Nature*, 2018, **559**, 547.

198 A. Aspuru-Guzik, R. Lindh and M. Reiher, *ACS Cent. Sci.*, 2018, **4**, 144.

199 A. Nandy, J. Zhu, J. P. Janet, C. Duan, R. B. Getman and H. J. Kulik, *ACS Catal.*, 2019, **9**, 8243.

200 B. Meyer, B. Sawatlon, S. Heinen, O. A. von Lilienfeld and C. Corminboeuf, *Chem. Sci.*, 2018, **9**, 7069.

201 R. García-Muelas and N. López, *Nat. Commun.*, 2019, in press.

202 Z. W. Ulissi, A. J. Medford, T. Bligaard and J. K. Nørskov, *Nat. Commun.*, 2017, **8**, 14621.

203 K. Tran and Z. W. Ulissi, *Nat. Catal.*, 2018, **1**, 696.

204 C. Rudin, *Nat. Mach. Intell.*, 2019, **1**, 206.